JOURNAL OF AIRCRAFT
Vol. 46, No. 1, January–February 2009

Flow Control of an Airfoil via Injection and Suction

T. L. Chng*
National University of Singapore,
Singapore 119260, Republic of Singapore
and
A. Rachman, H. M. Tsai,† and Ge-Cheng Zha‡
University of Miami, Coral Gables, Florida 33124

DOI: 10.2514/1.38394

We report on an experimental study of a Clark-Y airfoil subjected to both flow injection and suction in the manner of the coflow-jet flow control method. The study was conducted at Reynolds numbers of 7.4×10^4 and 1.3×10^5 for three different jet momentum coefficients: $C_\mu = 0.02$, 0.04, and 0.16. Some numerical computations are used to assess the extent to which they are adequate for engineering analysis and design of the coflow-jet method. The results clearly demonstrate the lift augmentation capability, particularly at high incidence angles. The increase in lift and stall margin depends on the momentum coefficient, and for the range tested, the increase in the integral of the airfoil static pressure distribution varies from 40 to 100%. The results suggest that the coflow-jet airfoil is more effective when both injection and suction are used simultaneously, compared with the case in which they are individually used. A first-order analysis of the combined merits of injection and suction indicate that these processes are not strongly coupled to each other and thus may possibly be analyzed separately.

Nomenclature

b	=	airfoil span
C_p	=	static pressure coefficient $[(p_s - p_\infty)/0.5\rho_\infty V_\infty^2]$
C_μ	=	jet momentum coefficient $(\dot{m}_j V_j/0.5\rho_\infty V_\infty^2 S)$
c	=	airfoil chord
$\dot{m}_j$	=	jet mass flow rate
p_s	=	airfoil static pressure
p_{tot}	=	total pressure
p_∞	=	freestream static pressure
Q	=	volumetric flow rate
Re	=	Reynolds number $(\rho_\infty V_\infty c/\mu)$
V_j	=	jet injection bulk velocity
V_∞	=	freestream velocity
S	=	projected wing area $(b \times c)$
x	=	chordwise axis
z	=	spanwise axis
α	=	angle of attack
μ	=	freestream dynamic viscosity
ρ_∞	=	freestream density

I. Introduction

ACTIVE flow control has been envisaged as a potential means of exceeding the aerodynamic performance limits of a conventional aircraft wing [1]. By controlling the flow over the wing, both the stall margin and/or the maximum lift coefficient can be increased. The upshot is an enhancement in the takeoff and landing capability of the aircraft or the option of a reduction in wing area. Furthermore, such techniques may achieve an augmentation in lift with an attendant increase in the lift-to-drag ratio and therefore lead to an added benefit of greater fuel economy.

Received 13 May 2008; accepted for publication 21 September 2008.

*Associate Scientist, Temasek Laboratories, 10 Kent Ridge Crescent. Member AIAA.
†Member AIAA.
‡Associate Professor, Department of Mechanical and Aeronautical Engineering. Senior Member AIAA.

Examples of active flow control concepts in the nascent stages of implementation include circulation control (CC) by blowing while concurrently exploiting the Coanda effect [2–5] and the use of either continuous suction or blowing on an airfoil surface [1,6,7]. Such active flow control concepts essentially involve imparting momentum to the flow, which requires energy expenditure that can impact the overall efficiency of the system. There is also a potential thrust penalty incurred due to the ejected mass flow. In the hope of improving efficiency, researchers have proposed concepts such as the use of pulsed jets [8,9] and net-zero-mass-flux synthetic jets as a more efficient substitute for continuous jets [4]. However, such techniques have not gained practical use, as their overall effectiveness in augmenting lift and stall margin is relatively limited [10].

The present study deals with the concept of applying a coflow jet (CFJ) on an airfoil as suggested by [2,11–13]. The idea entails the creation of a wide spanwise slot on the airfoil suction (upper) surface, as shown in Figs. 1 and 2. High-speed fluid is expelled tangentially to the airfoil surface through an injection port near the leading edge, and an identical amount of mass flow is simultaneously withdrawn via a suction port located near the trailing edge. The turbulent shear layer between the main flow and the jet causes strong turbulence diffusion and mixing, which enhances lateral transport of energy from the jet to the main flow and allows the main flow to overcome the adverse pressure gradient responsible for flow separation at high incidence angles.

The novelty of this approach lies in the recirculation of the fluid, which leads to increased efficiency, because the penalty of dumping the injected fluid is avoided through the net-zero-mass-flux arrangement. Additionally, the orientation of the slot on the suction surface ensures that the momentum transfer occurs tangentially to the airfoil surface. This eliminates the necessity of having a thick trailing edge, which is otherwise crucial in CC techniques that use the Coanda effect. The CFJ concept can thus be applied to airfoils of virtually any geometry, and its potential superior efficiency implies that it can be employed within the entire flight envelope. To date, wind-tunnel tests have been conducted on a relatively thick airfoil out of practicality in implementing suction and blowing in the test model. Using a NACA0025 CFJ airfoil, Zha et al. [2] have demonstrated the viability of this technique. With the momentum coefficient varying from 0.1 to 0.3, the maximum lift coefficient and stall margin were found to increase by between 113–220 and 100–153%, respectively. For lower momentum coefficients within 0.055

to 0.192, a reduction in drag ranging from 30 to 127% compared with the baseline airfoil could also be achieved.

It is also shown that the mass flow rate of the recirculated fluid displays a direct relationship with the lift coefficient and the stall margin up to a certain threshold value [2]. Beyond this limit, any further increase leads to deterioration in aerodynamic performance due to instability of the injected wall jet fluid. Two possibilities have been put forward to explain this behavior: the large disparity between the Mach number of the jet and the freestream results in instabilities in the mixing shear layer, and the centrifugal force of the jet becomes so large that the injected flow does not exit tangentially to the airfoil surface. In another study, the enhancement in circulation with suction conducted in tandem with injection was found to be significantly superior to the case in which only injection was used [13]. This implies that the advantage of the CFJ concept may not simply be limited to an increase in aerodynamic efficiency but can also achieve an augmentation in lift and stall margin and a reduction in drag when compared with other existing techniques.

The aim of this study is to investigate the performance of the CFJ concept as applied to a Clark-Y airfoil, which is approximately half the thickness of that in previous studies, at high angles of attack and at different mass flow rates. The Clark-Y is also a low-speed airfoil commonly used in aircraft modeling with benign stall characteristics and is typical of the class of airfoils suited for application on unmanned aerial vehicles. The performance of the modified Clark-Y airfoil (henceforth termed the CFJ airfoil) with pure injection and pure suction is also examined. Unlike earlier studies on the CFJ airfoils in which the performances are assessed via force measurements, in the present experimental study, detailed surface pressure distributions are measured. Computations of the CFJ airfoil are also made to assess if they can produce a level of accuracy suitable for engineering analysis. The remainder of this paper is organized as follows: Secs. II and III, respectively, present details of the experiment and computation. and Sec. IV provides a discussion of the test results.

II. Experimental Setup

A. Airfoil Geometry and Jet Injection and Suction System

The baseline airfoil adopted in this study is the Clark-Y airfoil with a 12% chord thickness and is selected for its simple yet robust design.

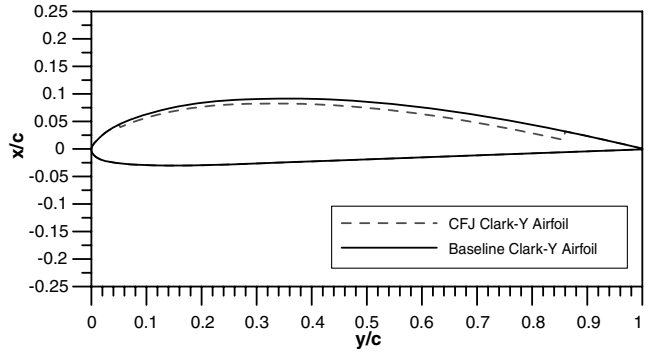

Fig. 1 Baseline and CFJ Clark-Y airfoil geometry.

A geometric comparison between the baseline and CFJ Clark-Y airfoils is shown in Fig. 1. Note that the dotted line shows the wide spanwise slot removed from the baseline airfoil to form the CFJ airfoil. Both airfoils have a chord c of 210 mm and a span b of 390 mm and are similar in geometry, apart from the mentioned slot on the suction surface of the CFJ model. Both test models were fabricated via a rapid prototyping process using Objet Full Cure-700 photopolymer material and then polished to ensure a good surface finish.

The internal cross-sectional geometry of the CFJ airfoil is shown in Fig. 2. A total of 38 static pressure taps were located along the midspan of the baseline airfoil, of which 21 were located on the upper (suction) surface and 17 were on the lower (pressure) surface. The CFJ airfoil has 36 static pressure taps, consisting of 19 and 17 holes on the suction and pressure surfaces, respectively. Holes were created through the skin of the airfoil models to facilitate measurements from these pressure taps. Further, as a test for two-dimensionality of the flow, both models have 2 spanwise pressure taps located at ± 62 mm ($\pm 0.34b$) from the midspan at a chordwise location of $x/c = 0.7$ and 0.4 for the baseline and CFJ airfoils, respectively.

A large proportion of the internal volume of the CFJ model was hollow to provide ample space for the internal ducts. The injection exit height of the CFJ airfoil was 1.28 mm ($0.006c$) chord and it was located 11.00 mm ($0.052c$) from the leading edge. The suction inlet has a height of 3.35 mm ($0.016c$) and is located 180 mm ($0.86c$) from the leading edge. The height of the suction inlet was about thrice that of the jet inlet to remove an equal amount of mass flow that is being injected without choking the flow [2,11].

The extreme pressures within the internal ducts of the CFJ airfoil raise the possibility that the airfoil surface may deflect or deform during the process of fluid injection and suction. In view of this, 20 vertical support pillars were included within the internal duct of the CFJ model to minimize these effects. Furthermore, four steel rods extending across the airfoil span were inserted at various chordwise locations through the thickness of the airfoil polymer material to increase its structural rigidity. The locations of the support pillars and steel rods are also shown in Fig. 2.

The internal injection and suction ducts reside in separate fore and aft chambers, respectively, with each duct originating from opposite sides of the airfoil span. Studies have shown that attaining spanwise uniformity of both the injected and ingested fluids becomes more challenging if the blowing and suction lines are connected only on one side [14]. This being the case for the present system, additional measures were taken to ensure adequate spanwise uniformity. For instance, Fig. 2 shows that the injection and suction ducts were routed such that the fluid has to negotiate a turn at the respective inlets and outlets. This has been shown by Paxton et al. [14] to be an effective way of producing spanwise uniformity. In addition, two cylindrical metal pipes (one for injection and one for suction) with small holes drilled perpendicularly to their axes were inserted within the internal ducts to minimize the spanwise pressure gradient of the flow. Both of these pipes occupied the entire span of the CFJ airfoil and were sealed at one end to prevent air leakage. A priori tests were also conducted to ascertain the diameter and distribution of these holes that would produce an acceptable level of uniformity. For the circular-shaped pipe inserted within the injection duct, 38 holes

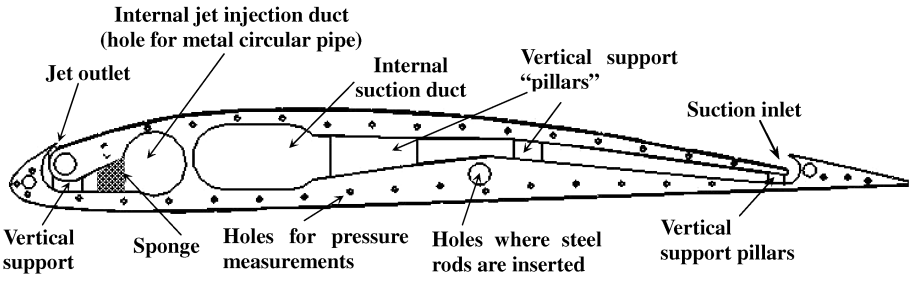

Fig. 2 A schematic of the CFJ airfoil internal cross-sectional geometry.

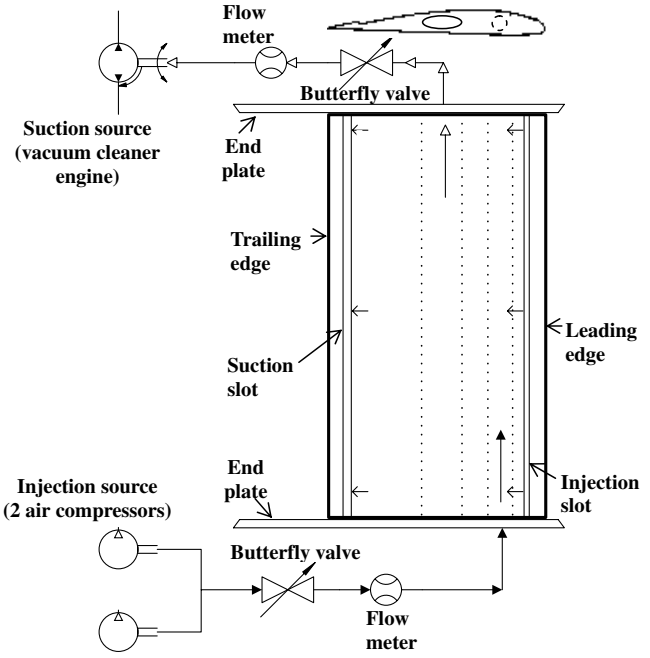

Fig. 3 Schematic of the jet injection and suction system. (Filled arrows depict the injection line and hollow arrows the suction line.)

spaced equally apart by a distance of 10 mm and each having a diameter of 1 mm was found to be an acceptable combination. For the oval-shaped pipe inserted within the suction duct, 60 holes were chosen, each having a diameter of 1.5 mm. The locations of these holes were such that they did not coincide with the vertical support pillars. Finally, a layer of sponge was inserted just after the circular pipe within the internal injection duct to provide a baffle that improves the flow uniformity (see Fig. 2). Two circular acrylic end plates with a thickness of 3 mm and a diameter of 340 mm were mounted on both sides of the airfoil span to avoid the interference of end effects.

A schematic of the CFJ airfoil and the injection and suction system is shown in Fig. 3. The injection source was represented by two air compressors connected in parallel, and the suction was provided by a 2000 W conventional vacuum cleaner. The volumetric flow rate of both lines was regulated by the use of butterfly valves and monitored via two separate Key Instruments FR4700 flow meters. Each flow meter had a measurement range of 150 to 1500 liter/min (lpm).

B. Wind-Tunnel Setup

Experiments were conducted in a low-speed open-loop wind-tunnel facility located at Temasek Laboratories, National University of Singapore. The wind tunnel has a test section with a square cross section of 450 by 450 mm and a length of about 1.3 m. The facility shows a turbulence intensity of about 0.4% within the range of velocities tested. With the airfoil mounted vertically in the test section, the geometric blockage varied between 5.6 to 19%, depending on the angle of attack. No attempts were made here to correct the acquired data due to blockage effects, as the standard available methods were found to produce negligible differences.

The freestream velocity was obtained with a pitot tube and a static pressure tap flushed with the tunnel wall located at 180 and 240 mm from the start of the test section, respectively. All pressure readings were acquired using a SETRA 265 differential pressure transducer with a range of 0 to 2.5 in H_2O. The pressure transducer was connected to a National Instruments PCI-6014 16-bit data acquisition card with a sampling rate of up to 200 kS/s installed on a Pentium IV PC. Mean airfoil pressure measurements were obtained by acquiring data at a sampling frequency of 100 Hz for a period of 30 s. These conditions were in line with the rated response time of the transducer and were found to be sufficient to produce a set of statistically stationary data.

C. Test Conditions

The main parameter investigated in this study is the mass flow rate, typically described by the momentum coefficient:

$$C_\mu = \frac{\dot{m}_j V_j}{0.5\rho_\infty V_\infty^2 S} \tag{1}$$

where $\dot{m}_j$ is the jet (or suction) mass flow rate; V_j is the bulk velocity of the jet; S is the projected wing area; ρ_∞ and V_∞ are the freestream density and velocity, respectively; and C_μ is defined with respect to the injection process and three different values ($C_\mu = 0.02, 0.04$, and 0.16) were tested. Note that if the suction velocity was used as the defining kinematic quantity in the numerator, the resulting value of the momentum coefficient would be reduced by a factor of about 2.6. This is due to the larger height of the suction inlet.

An important aspect of the CFJ concept is the equivalence of the mass flow rate for the injected and withdrawn fluid. In the present study, it should be noted that this fluid was not recirculated, but rather provided by two separate sources. Because the jet and freestream Mach number were both less than 0.3, the effects of compressibility were comfortably neglected, and an equivalent mass flow rate was achieved by maintaining an identical volumetric flow rate Q for both processes.

Tests were performed at two freestream velocities, $V_\infty = 5.4$ and 9.8 m/s, which gave chord-based Reynolds numbers Re of 7.4×10^4 and 1.3×10^5, respectively. The lower freestream velocity experiments were included to investigate the performance of the CFJ airfoil at higher momentum coefficients. Ideally, this could have been accomplished by increasing the volumetric flow rate, but the limited capacity of the available injection source precluded this possibility. However, conducting a section of the experiments at a lower freestream velocity also meant that a preliminary gauge of the Reynolds number effect could be observed. For all cases, two steel tubings with a diameter of 1 mm were placed at a chord wise location of about 2 mm ($0.01c$) from the leading edge on the top and bottom surfaces of the airfoil to act as trip wires that turbulate the flow.

To investigate the relative merits of simultaneous blowing and suction, experiments in which either one or both of these processes were absent were also performed. In addition, tests were also conducted to ensure adequate spanwise uniformity of the injection velocity. These tests were conducted in the absence of any freestream velocity and at the same volumetric flow rates of the actual experiments. The test matrix of the present study is provided in Table 1.

D. Two-Dimensionality Test

The uniformity of the pressure coefficient C_p at selected spanwise locations (only three ports are available) for a fixed chordwise position was used as a gauge of the freestream uniformity and is presented in Fig. 4. The absence of any distinct spanwise gradient of the pressure coefficient is a good indication that the freestream is relatively uniform.

To ascertain the level of spanwise uniformity of the jet injection, a pitot tube installed at about an angle of 30 deg from the chordwise x axis was traversed across the entire length of the injection slot. The presence of the internal duct curvature inevitably results in a nonuniform static pressure and thus can cause a velocity variation across the jet injection outlet. However, considering the scale of the test model, directly measuring the jet velocity from a 1 mm slot was deemed to be neither practical nor accurate. The ratio of the total pressure and the corresponding dynamic pressure presented in Fig. 5 are used as a measure of the spanwise uniformity. The nominal jet velocity V_j used in computing the jet dynamic pressure was based on the uniform bulk velocity of the jet (i.e., volumetric flow rate/area of injection outlet). Note that the pitot tube was located about 2 mm from the injection slot and data collection was restricted to $\pm 40\%$ from the airfoil midspan. The results show that the current setup yields a jet nonuniformity of about 5%.

Table 1 Test matrix of the present study

Test model	Volumetric flow rate, lpm	V_∞, m/s	V_j, m/s	C_μ	α, deg	Remarks
Baseline	0	5.4	NA	NA	0, 4, 8, 12, 16, 20	NA
Baseline	0	9.8	NA	NA	0, 4, 8, 12, 14, 16, 18, 20	NA
CFJ	0	5.1	0	0	0, 8, 12, 14, 16	NA
CFJ	0	9.8	0	0	0, 8, 10, 12, 14, 16, 18, 20	NA
CFJ	400	9.8	13.1	0.02	0, 8, 10, 12, 14, 16, 20	Injection, suction
CFJ	550	9.8	18.1	0.04	0, 8, 12, 14, 16, 18, 20	Injection, suction
CFJ	300	5.6	9.9	0.04	0, 8, 12, 14, 16, 18, 20	Injection, suction
CFJ	550	5.1	18.1	0.16	0, 8, 12, 16, 18, 20, 22, 24	Injection, suction
CFJ	550	9.8	18.1	0.04	0, 8, 12, 14, 16, 18, 20	Injection
CFJ	550	9.8	18.1	NA	0, 8, 12, 14, 16, 18, 20	Suction
CFJ	550, 400, 300	0	18.1, 13.1, 9.9	NA	0	Injection
CFJ	550, 400, 300	0	18.1, 13.1, 9.9	NA	0	Suction

E. Experimental Uncertainty

The main sources of uncertainty stem from the flow meters used to measure the flow rate of the injected and ingested fluids as well as the pressure transducer used to record the pressure data. The former have an accuracy rating of 3% full scale, or 45 lpm. This translates into an uncertainty of 1.5 m/s in terms of velocity and thus an uncertainty of between 8 to 15% for V_j. The pressure transducer has an accuracy of 1% full scale, or 0.025 in H_2O.

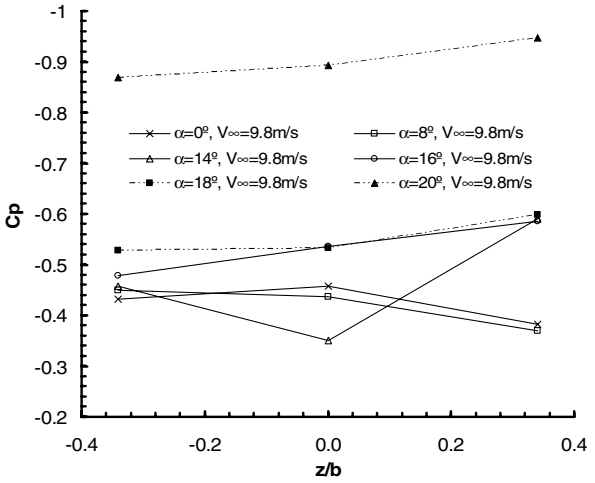

Fig. 4 Spanwise distribution of the pressure coefficient obtained at $x/c = 0.7$ for the baseline airfoil at various angles of attack.

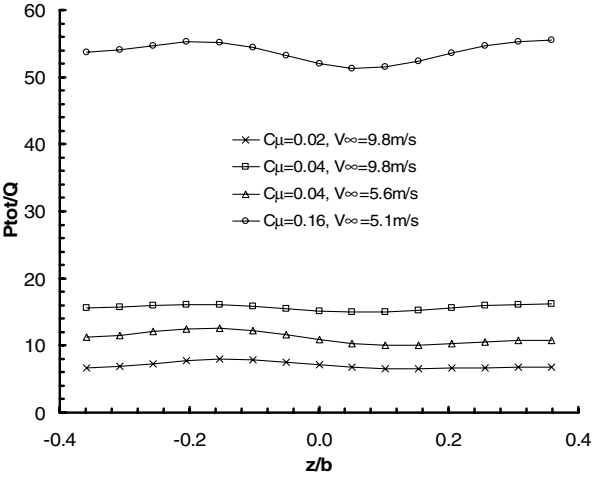

Fig. 5 Spanwise distribution of total pressure as an illustration of the jet uniformity.

III. Computational Analysis

Computations were performed using a commercial computational fluid dynamics (CFD) software, FLUENT, to establish if a simple Reynolds-averaged Navier–Stokes (RANS)-type computation provides acceptable accuracy for engineering studies. Though it is recognized that the CFJ concept involves the relatively more complex subset of wall jets, previous studies indicate that there is currently no clear choice of turbulence RANS model that can accurately simulate such a problem [15,16]. Furthermore, evaluating and validating such computations would invariably involve detailed experimental data that include high-order turbulence measurements that are beyond the scope of the present study.

A non-time-accurate 2-D simulation with a one-equation Spalart–Allmaras turbulence model commonly employed for external aerodynamic analysis was used. Studies with different grid resolutions were initially made to ensure that the grid used was sufficiently adequate for this problem. The final grid for the CFD simulation is shown in Fig. 6 and consists of 22,000 cells for the baseline Clark-Y airfoil and 25 000 cells for the CFJ airfoil to achieve a balance between turnaround time and accuracy. The grid resolution for the Clark-Y case was the amount commonly used to resolve low-speed airfoils and no further elaboration is provided. The wall jet outlet and the suction-inlet region of the CFJ airfoil, as shown on Fig. 6c, has a high concentration of grid points, typically about an additional 3000 grid points, to resolve the layer from the wall to the height of the respective slots. The computational domain for both airfoils encompasses a radius of $30c$. Time-averaged results are presented in instances in which unsteady flow separation and vortex shedding occur.

The boundary conditions of the jet injection and suction were simulated with a mass inlet and pressure outlet condition, respectively. The injected flow and ingested flow are both assumed to be perfectly uniform and perpendicular to their corresponding exit and inlet planes. Possibly, a more realistic model would be to include both the internal injection and suction ducts, but at the expense of longer computations. A uniform velocity at the injection outlet is thus used for simplicity and practicality. The test matrix for the computational cases is similar to those listed in Table 1, but with less emphasis on cases within the poststall regime, due to the poorer predictive capability for stall with the current RANS model used.

IV. Results and Discussion

The integral of the static pressure coefficient around the airfoil surface for the CFJ airfoil model for various conditions is presented in Figs. 7–11. Attempts for direct measures of the lift and drag coefficient for the CFJ airfoil were also made, but as the interference of the pressure and suction ducts with the load measurements in the experimental setup were significant, they are not sufficiently reliable for inclusion here. Instead, the integral of the static pressure mentioned previously is employed as a means of estimating the lift variation with a change in angle of attack. As experimental pressure

data were only measured at the airfoil midspan, this integrated quantity only represents the sectional lift increase attributable to the pressure forces acting normal to the surface at the midspan. This quantity does not, therefore, account for the forces generated at the injection outlet and suction inlet. However, the static pressure measurements and their integral value will give us an idea of the influence of the CFJ concept in controlling the flow over the airfoil.

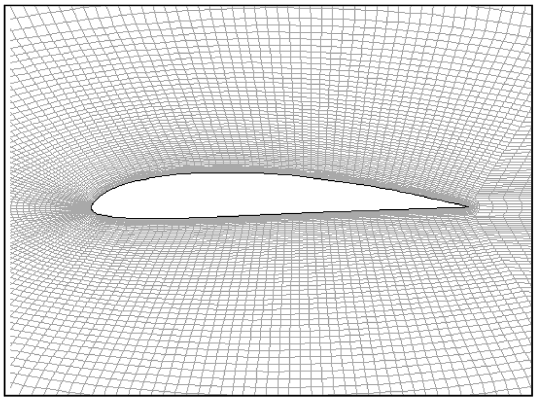

a)

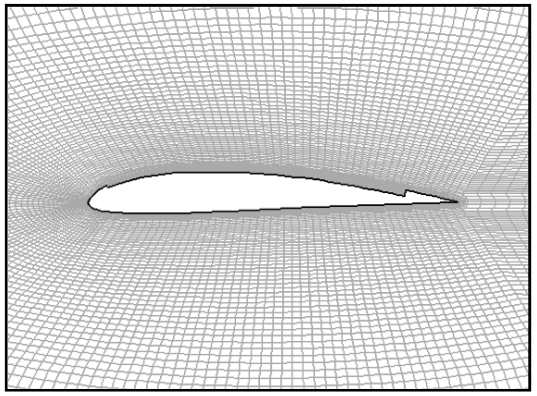

b)

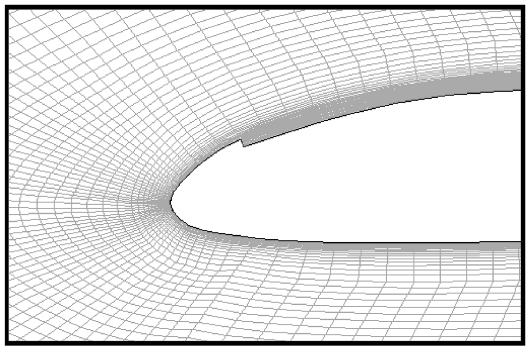

c)

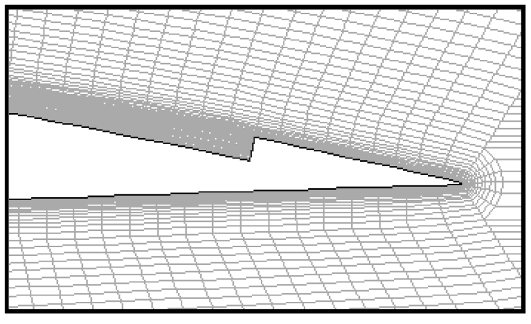

d)

Fig. 6 Grid distribution for a) baseline Clark-Y airfoil, b) CFJ airfoil, c) magnified view in the vicinity of the jet exit, and d) magnified view in the vicinity of the suction inlet.

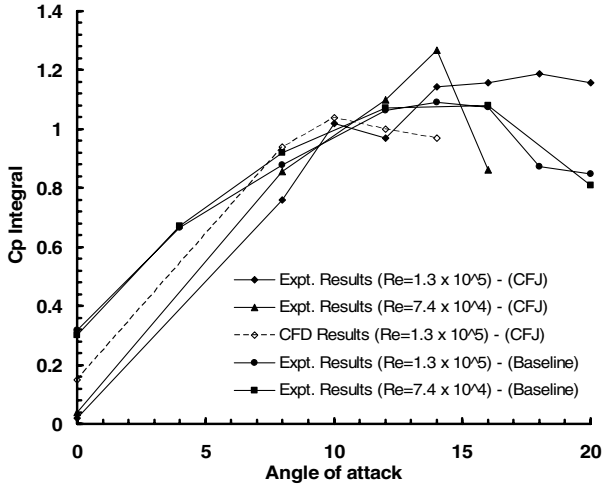

Fig. 7 Variation in the static pressure integral with α for the CFJ airfoil at $C_\mu = 0$ and $V_\infty = 5.1$ and 9.8 m/s.

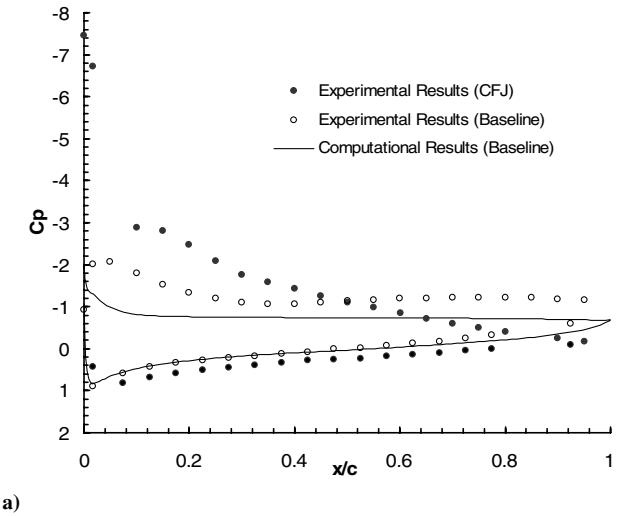

a)

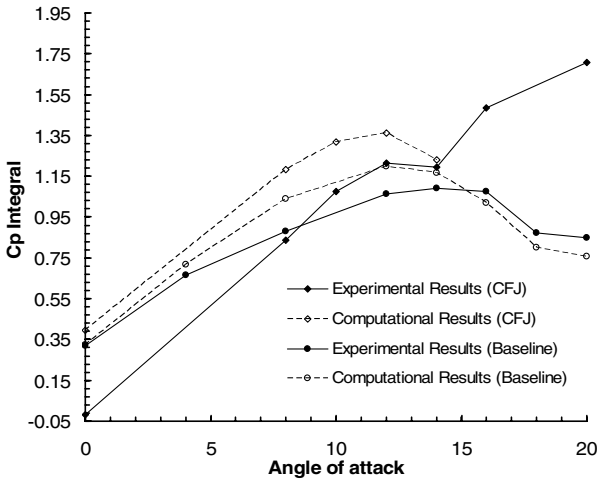

b)

Fig. 8 Plots of a) pressure coefficient distribution of the CFJ airfoil at $C_\mu = 0.02$, $V_\infty = 9.8$ m/s, and $\alpha = 20$ deg and b) variation in the static pressure integral with α for the CFJ airfoil at $C_\mu = 0.02$ and $V_\infty =$ 9.8 m/s.

When applicable, the experimental and computational data for the baseline airfoil are also included for comparison. As the emphasis of our investigation is on high angles of attack, surface static pressure measurements were made at several incidence angles ($\alpha = 0$, 8, 14, 16, and 20 deg). Experiments were conducted at two different Reynolds numbers ($Re = 7.6 \times 10^4$ and 1.3×10^5), but computations were made only at the higher Reynolds number.

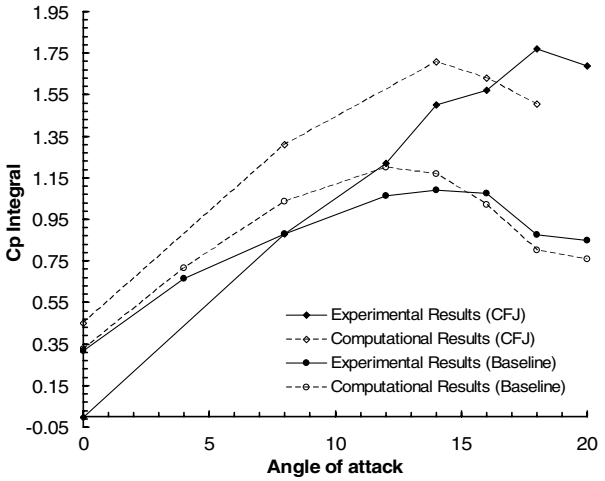

Fig. 9 Variation in the static pressure integral with α for the CFJ airfoil at $C_\mu = 0.04$ and $V_\infty = 9.8$ m/s.

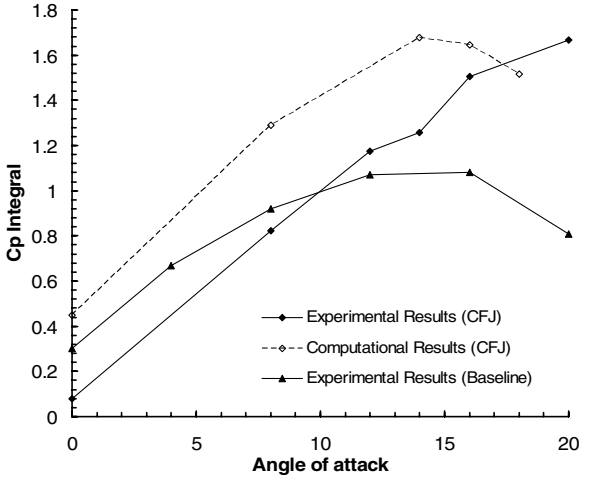

Fig. 10 Variation in the static pressure integral with α for the CFJ airfoil at $C_\mu = 0.04$ and $V_\infty = 5.6$ m/s.

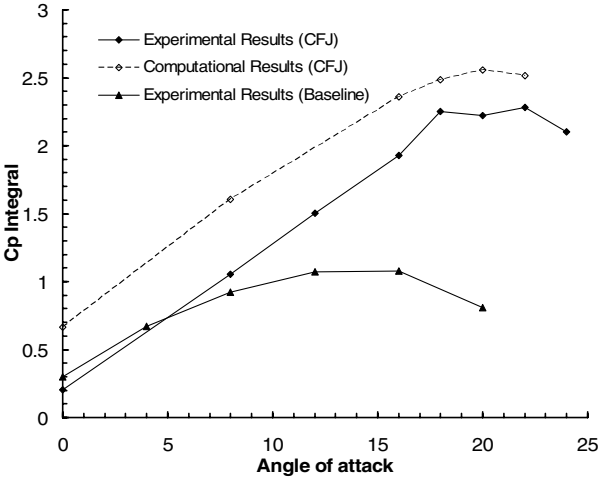

Fig. 11 Variation in the static pressure integral with α for the CFJ airfoil at $C_\mu = 0.16$ and $V_\infty = 5.1$ m/s.

A. Effects of Simultaneous Injection and Suction

1. $C_\mu = 0$ (No Injection and Suction), $V_\infty = 5.1$ and 9.8 m/s

As noted, the CFJ airfoil is created by modifying the upper surface of the Clark-Y airfoil. The manner of the CFJ airfoil modification is conceived such that it performs optimally with both injection and suction in operation. However, to assess the geometric modifications on the airfoil performance, measurements in the absence of blowing and suction are compared with the baseline Clark-Y airfoil. Results show that although the pressure distribution on the lower surface does not display significant variations, the differences on the upper surface are very apparent. Figure 7 shows that the static pressure integral is visibly lower than that of the baseline at angles of attack below 8 deg. The CFJ airfoil also experiences a lower stall angle when injection and suction are both absent. However, at higher incidence angles, particularly when both airfoils experience flow separation, this negative effect on the lift is diminished and the C_p integral for both the CFJ and baseline airfoils becomes comparable. Although the changes in the C_p integral of the CFJ airfoil can probably be attributed to the presence of the spanwise injection slot, the exact response to this uneven geometry varies with the angle of attack. It is possible that the uneven geometry serves to initiate flow separation at lower incidence angles but promotes flow mixing and transition at higher angles of attack. Examples of both types of behavior have been reported in [2,17], respectively. Given that the locations and sizes of the injection boundaries were relatively different in both studies, this suggests that the lift response for such flow control techniques could be significantly affected by these geometric parameters or modifications.

The computational results project an even poorer representation of the generated lift. From Fig. 7, the CFJ airfoil is seen to give lower values of the C_p integral at all angles of attack. Given the preceding, one of the drawbacks of the CFJ concept is that continuous operation would possibly be a vital requirement, especially at angles of attack below 8 deg. At these operating angles particularly, any disruption may be at the expense of a drastic degradation in performance. As an extreme example, one should note that from the experimental data, almost no lift is produced when $\alpha = 0$. This implies that the positive effect of airfoil camber is totally negated by the uneven geometry.

2. $C_\mu = 0.02$ and $V_\infty = 9.8$ m/s

As expected for this case, the presence of injection and suction mainly affects the airfoil suction surface, resulting in an upward shift of the C_p curve (i.e., increased suction), as compared with the baseline Clark-Y airfoil, particularly for the higher incidence angles. The pressure distribution on the bottom surface remains relatively unchanged. The additional momentum imparted by the external fluid accelerates the flow above the entire airfoil suction surface, which causes an increase in lift. By way of example, it is apparent for the case of $\alpha = 20$ deg in Fig. 8a that flow separation present in the baseline case has effectively been inhibited with the introduction of the external fluid. The stagnation point on the bottom surface (i.e., where $C_p = 0$) has moved further downstream and the C_p distribution indicates that the flow remains attached on the suction surface. The profile of this pressure plot is also typical of the flow-separation-delay behavior described in the cases that follow.

Figure 8b shows a comparison of the static pressure integral for the CFJ and baseline airfoils. The experimental results indicate an increase in this quantity for incidence angles above $\alpha = 8$ deg by as much as 40%. When the angle of attack is low, the increase in lift is balanced out by the deterioration in performance caused by the presence of the wide spanwise slot, as mentioned previously. However, with further increase in α, an enhancement in lift in excess of the baseline value can be achieved. The dissimilarity in gradients of the pressure integral curves can be attributed to the different geometries of both airfoils. The improvement in the stall margin is a direct consequence of the flow separation being suppressed at high angles of attack.

3. $C_\mu = 0.04$, $V_\infty = 9.8$ m/s, $C_\mu = 0.04$, *and* $V_\infty = 5.6$ m/s

The effects of a twofold increase in the jet momentum coefficient over the previous case and for two different freestream velocities are shown in Figs. 9 and 10. Similar observations to those described in the previous configuration are noted: namely, that of attached flow and an augmentation in lift at high angles of attack. This trend is consistent for both the CFD and experimental data. Only a marginal difference exists in the maximum value of the C_p integral. Similarly, the C_p integral is also not greatly affected by C_μ at lower angles of attack, especially when $\alpha = 0$ deg. On the other hand, the CFD results predict a rise in lift as C_μ is increased. The disagreement in these two groups of results is clearly illustrated by comparing the plots presented in Figs. 9 and 10 with those in Fig. 8b. For instance, the peak value of the C_p integral from the experimental curves in these 3 figures is approximately 1.7. However, from the computational results, a twofold increase in C_p (from 0.02 to 0.04) leads to a corresponding increase in the C_p integral from 1.35 to 1.7. This represents a more than proportionate magnitude of increase.

Notwithstanding this inconsistency in the computational and experimental data, it is otherwise noticed that when both sets of data are viewed individually, their C_p integral curves (see Figs. 9 and 10) are fairly similar with respect to freestream velocity. This may be a further indication that the freestream velocity or Reynolds number may not be a critical parameter in determining any consequent lift enhancement.

4. $C_\mu = 0.16$ *and* $V_\infty = 5.1$ m/s

An increase in the value of C_μ to 0.16 produces no discernible changes in the trend of the airfoil pressure distribution, as compared with the cases with lower momentum coefficients (see Fig. 11). Flow separation is suppressed, leading to lift enhancement at high incidence angles of up to $\alpha = 24$ deg, and the magnitude of the pressure integral rises to a maximum of about 2.3, as shown in the experimental curve. This represents a twofold increase over the baseline configuration and about a 35% improvement over the cases in which $C_\mu = 0.02$ and 0.04. In addition, the envelope within which there is an enhancement in lift compared with the baseline is also slightly larger; the crossover point shifts from $\alpha = 8$ to 5 deg. Figure 12b depicts the computed streamlines and Mach number contour plot of the flow at $\alpha = 20$ deg with $C_\mu = 0.16$. The streamlines are indicative of attached flow at this incidence angle and contrast with the separated flow exhibited in Fig. 12a for the baseline airfoil.

Figures 13a and 13b, respectively, show the variation of the static pressure integral with incidence angle at different momentum coefficients for the experimental and CFD results. Collectively, both sets of data indicate that even small values of the momentum coefficient on the order of 0.02 are able to deliver an improvement in lift, as compared with the baseline. It also appears that the Reynolds number has an insignificant effect on lift enhancement for the two values of V_∞ tested.

B. Sensitivity of the C_p Integral to Changes in the Momentum Coefficient

One of the observations drawn from the experimental data is that the Cp integral responds differently to changes in C_μ for different

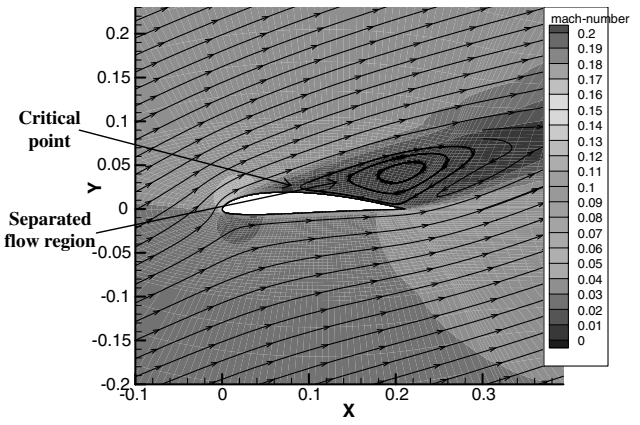

a)

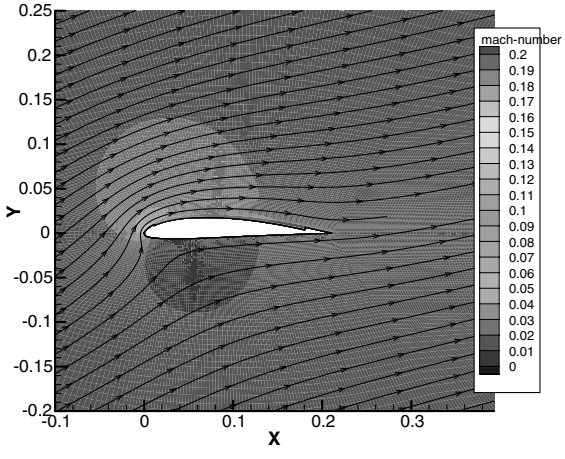

b)

Fig. 12 Mach number contour plot and streamlines at $\alpha = 20$ deg and $V_\infty = 5.1$ m/s for a) baseline Clark-Y airfoil and b) CFJ airfoil with $C_\mu = 0.16$.

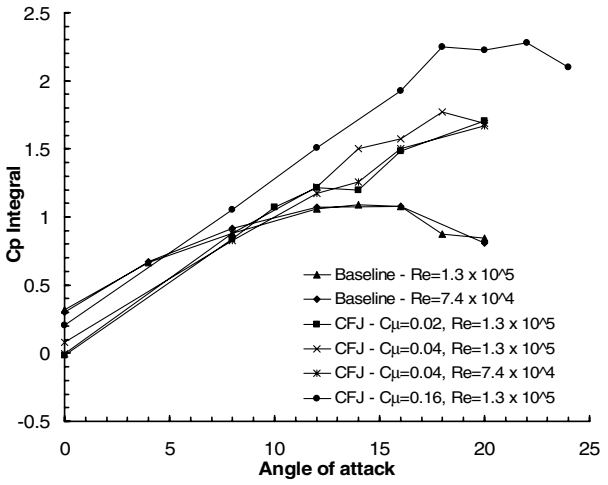

a)

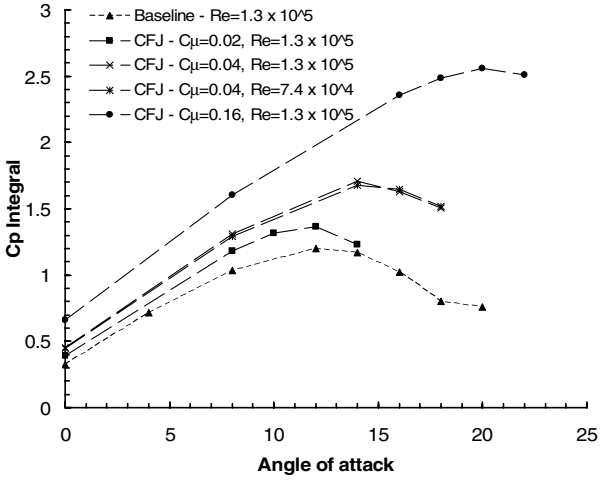

b)

Fig. 13 Variation in the static pressure integral with angle of attack for selected test cases: a) experiments and b) CFD simulations.

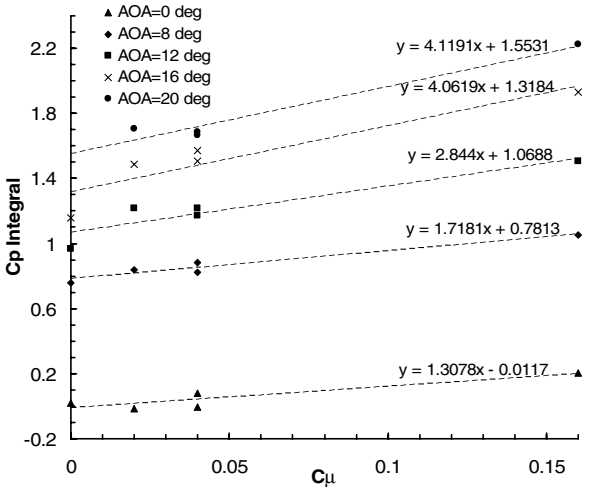

Fig. 14 Sensitivity of the C_p integral to changes in the momentum coefficient C_μ.

angles of attack. For a clearer understanding of this relationship, the variation of the C_p integral is plotted in Fig. 14 for different incidence angles. The gradients of the individual curves are seen to display a direct relationship with α. This is a reasonable indication that application of the CFJ concept would be less effective at lower angles attack. This also means that if a CFJ airfoil is required to yield superior performance, as compared with the baseline, for *all* angles of attack, a substantially higher momentum coefficient may be necessary. From a lift production standpoint, operation of a CFJ airfoil at higher angles of attack may thus be more desirable, provided that the stall angle at that particular momentum coefficient is not exceeded.

C. Comparison of Computational and Experimental Results

To compare the accuracy of the computations with the experiments, the airfoil pressure distributions for a momentum coefficient $C_\mu = 0.16$ are shown in Fig. 15. The results for this arbitrarily chosen value of 0.16 are found to be representative of the corresponding plots for the other momentum coefficients.

The principal observation is that the computational and experimental data are in reasonable agreement in terms of trend, though less so in terms of magnitude. The difference in the static pressure integral for both sets of data varies between 4 to 18%, depending on the specific angle of attack and momentum coefficient. The disparity is generally more pronounced at higher momentum coefficients and lower angles of attack, but it stems primarily from a difference in the corresponding values of the pressure coefficient on the airfoil suction surface (see Figs. 15a–15d), particularly in the vicinity of the injection and suction fluid boundaries. This could be due to the crude assumptions used in defining these boundary conditions.

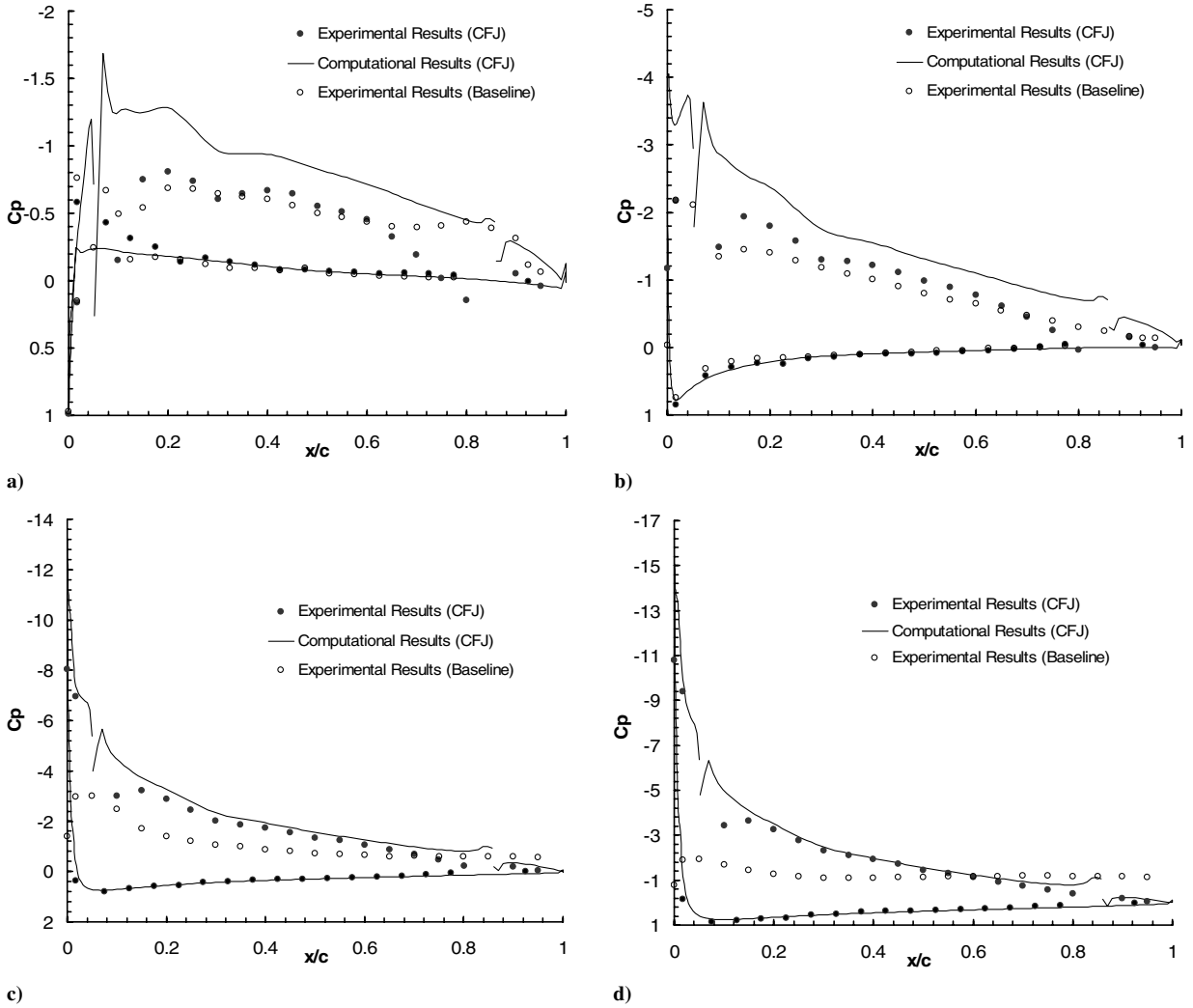

Fig. 15 Pressure coefficient distribution of the CFJ airfoil at $C_\mu = 0.16$ and $V_\infty = 5.1$ m/s: a) $\alpha = 0$ deg, b) $\alpha = 8$ deg, c) $\alpha = 16$ deg, and d) $\alpha = 20$ deg.

Another important dissimilarity (as can be noted from Fig. 13) is that the computational results fail to predict the sensitivity of the lift to the angle of attack observed in the experiments. Rather, the computations predict an increase in the C_p integral with C_μ at all angles of attack for the CFJ airfoil (i.e., an almost constant gradient for the respective surface loading curves) and also underpredict the stall margin. The latter is not unusual, however, and is expected to be related to the poorer predictive capability for stall by existing CFD methods.

Finally, the pressure distribution curves predicted by the simulations in Fig. 15 also show the presence of spikes near chordwise locations corresponding to the injection and suction boundaries. This phenomenon, which is especially evident in the computation, is observed for all cases in which blowing and suction are employed. The spikes are both in the downward direction and therefore result in a less negative value of C_p. The magnitude of the spike correlates directly with the velocity: because the geometry of the CFJ airfoil remained unchanged throughout, larger momentum coefficients led to larger spikes, and the spikes at the suction inlet were perpetually smaller in magnitude than those at the injection outlet. It is plausible that these features may be due to the omission of the internal ducts when modeling the injected and ingested flow. Because the pressure of the injected and ingested fluids is specified directly at the respective outlet and inlet of each process, the difference between the local pressure at these locations and that of the flow over the airfoil may thus account for the jump observed. Similar spikes were also observed in the CFJ airfoil surface isentropic Mach number plot in [11].

D. Effects of Employing Injection and Suction in Isolation

As seen earlier, the concept of the CFJ airfoil entails continuous operation of both the injection and suction process to improve performance. However, it is also useful (for example, in the possible event of failure of just a single process) to investigate the relative merits of each process. For this purpose, the lift curves for four different configurations are presented in Fig. 16. These configurations consist of the following: simultaneous injection and suction ($C_\mu = 0.04$), injection only, suction only, and the case in which injection and suction are absent (i.e., $C_\mu = 0$). The baseline case is also included for reference. Except for the last configuration, the flow rates for the injection and suction processes in the first three cases correspond to a constant value of 550 lpm. Admittedly, the presence of the uneven geometry due to the nonconformal injection and suction slots do not ensure an entirely fair comparison, but we believe that this will not invalidate our conclusions that follow.

Expectedly, both sets of results (see Figs. 16a and 16b) generally indicate that a combination of injection and suction outperforms the instances in which these processes are employed separately. When the lift-enhancement characteristics of these two individual processes differ, the use of fluid injection appears to be the better alternative. In fact, it is instructive that for the case in which only suction is employed, the CFD results even project a lower value of the C_p integral than with the baseline airfoil for $\alpha \leq 8$ deg, due to the strong possibility of upstream flow separation. Also of note is that although the preceding observations are generally true for all angles of attack as predicted by the CFD simulations, they are only valid for $\alpha \geq 8$ deg from the experimental data.

It is not entirely clear why fluid injection seems to be the more effective of the two processes, but this can probably be accounted for by the fact that the suction momentum coefficient is less than half that of the injection by virtue of the larger suction-inlet height. It is also likely that the suction is conducted in the vicinity of the trailing edge and thus has less effect on upstream flow separation near the leading edge. It should be borne in mind that one of the primary intentions of simultaneous blowing and suction is to create a region of higher momentum to overcome the adverse pressure gradient present: both blowing and suction energize the boundary layer.

Though it is apparent that simultaneous injection and suction is the most desirable configuration among the four preceding configurations, it is also interesting to consider the synergistic benefits of this arrangement. This is evaluated as follows: for each configuration in which either injection or suction is absent, the difference in the value of the static pressure integral, as compared with the case in which $C_\mu = 0$, is noted. A crude approximation is arrived at by adding this difference together for both cases (termed here as superimposed case) and comparing it to the actual case in which simultaneous blowing and suction was performed (i.e., $C_\mu = 0.04$). It turns out that a comparison between the actual and superimposed cases yields a reasonably consistent set of data (see Fig. 17). This first-order analysis suggests that to a certain degree, the injection and suction processes can be treated as mutually exclusive of each other and thus may possibly be analyzed separately.

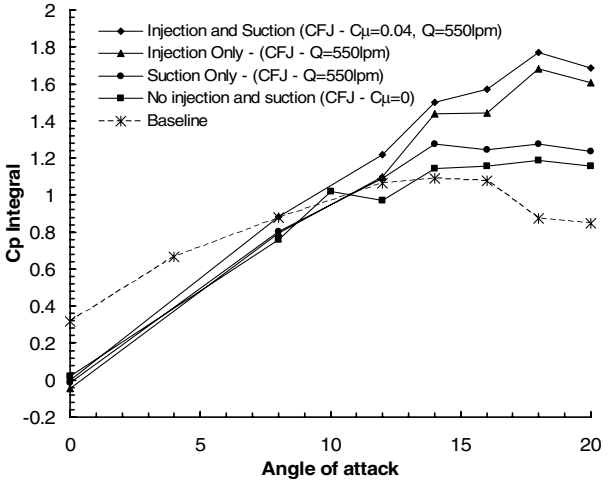

a)

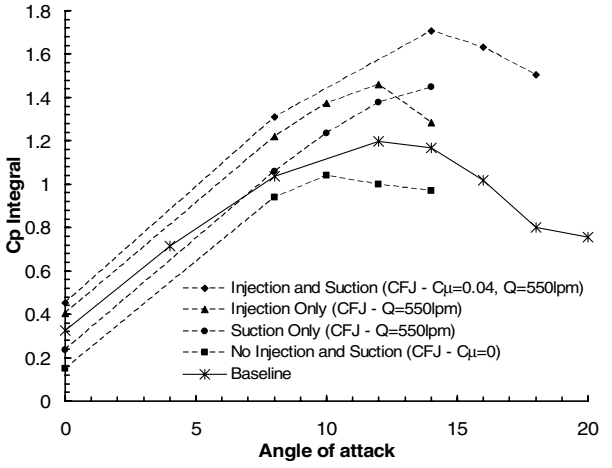

b)

Fig. 16 Variation in the static pressure integral with angle of attack for different combinations of injection and suction: a) experiments and b) CFD simulations.

VI. Conclusions

A study was conducted to assess the lift-enhancement capabilities of the CFJ concept and establish if these benefits extend to airfoils with typical relatively low thickness-to-chord ratio commonly used for low-speed flight applications. Wind-tunnel tests were conducted on an unmodified (baseline) Clark-Y airfoil and compared against that of an airfoil modified suitably to implement the CFJ concept. No attempts, however, were made to improve or optimize the CFJ airfoil geometry or jet coefficient needed.

Detailed static pressure data at the airfoil midspan were integrated to provide a reasonable indication of the sectional lift coefficient and

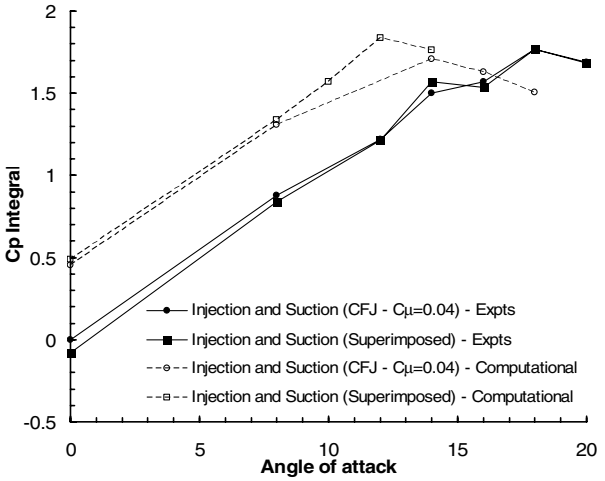

Fig. 17 Comparison of the synergistic merits of simultaneous injection and suction.

compared against numerical predictions using the Spalart–Allmaras turbulence model to assess the extent to which they are adequate for engineering analysis and design. The computations reflect the experimentally observed effects of the momentum coefficient C_μ on the static pressure integral.

The present study indicates that the current computational approach can be used to explore the design of CFJ airfoils in terms of determining the more critical parameters relevant to different objectives such as lift enhancement. Experiments are nonetheless necessary to valid the outcome of such design studies.

For a fixed value of C_μ, a variation in the freestream velocity (viz., Reynolds number) has an insignificant impact on the lift, at least for the very limited speed range tested here. On the other hand, the momentum coefficient shows a direct relationship with the static pressure integral. From the experimental data, a remarkable increase in lift of about 40% is observed even at the lowest momentum coefficient of $C_\mu = 0.02$, and this improvement extends up to approximately 100% when $C_\mu = 0.16$. These figures are 15 and 144%, respectively, as predicted by the CFD results.

Based on the experimental results, it is observed that the lift is less sensitive to changes in the momentum coefficient at lower angles of attack. The effect of the CFJ concept is pronounced at higher angles of attack in extending the stall margin of the airfoil.

The use of injection and suction in tandem outperforms the configurations in which either one or both of these processes were absent. Of the two processes, it appears that there is greater lift augmentation derived from jet injection than with suction. When compared against the baseline Clark-Y airfoil, it is noted that the CFJ configuration with pure injection performs only marginally better, whereas the corresponding case without injection yields poorer performance at lower angles of attack. This implies that using either injection or suction in isolation may require a higher C_μ to prove to be effective. An evaluation of the synergistic merits of injection and suction interestingly reveals that both of these processes are not strongly coupled to each other. This raises the possibility that they may be analyzed separately.

References

[1] Sellers, W. L., III, Singer, B. A., and Leavitt, L. D., "Aerodynamics for Revolutionary Air Vehicles," 21st AIAA Applied Aerodynamics Conference, AIAA Paper 2003-3785, June 2003.

[2] Zha, G. C., Carroll, B. F., Paxton, C. D., Conley, C. A., and Wells, A., "High Performance Airfoil Using Co-Flow Jet Flow Control," *AIAA Journal*, Vol. 45, No. 8, 2007, pp. 2087–2090. doi:10.2514/1.20926

[3] Sellars, N. D., Wood, N. J., and Kennaugh, A., "Delta Wing Circulation Control Using the Coanda Effect," AIAA 1st Flow Control Conference, AIAA Paper 2002-3269, June 2002.

[4] Cagle, C. M., and Jones, G. S., "A Wind Tunnel Model to Explore Unsteady Circulation Control for General Aviation Applications," 22nd AIAA Aerodynamic Measurement Technology and Ground Testing Conference, AIAA Paper 2002-3240, June 2002.

[5] Jones, G. S., and Englar, R. J., "Advances in Pneumatic-Controlled High-Lift Systems Through Pulsed Blowing," 21st AIAA Applied Aerodynamics Conference, AIAA Paper 2003-3411, June 2003.

[6] Baker, W. J., and Paterson, E. G., "Simulation of Steady Circulation Control for the General Aviation Circulation Control (GACC) Wing," *Applications of Circulation Control Technologies*, Progress in Aeronautics and Astronautics, Vol. 214, AIAA, Reston, VA, 2006, pp. 513–538.

[7] Moeller, E. B., and Rediniotis, O. K., "Hingeless Flow Control over a Delta Wing Planform," 38th AIAA Aerospace Sciences Meeting and Exhibit, AIAA Paper 2000-117, Jan. 2000.

[8] McManus, K., and Magill, J., "Airfoil Performance Enhancement Using Pulsed Jets Separation Control," AIAA 4th Shear Flow Control Conference, AIAA Paper 97-1971, June 1997.

[9] Johari, H., and McManus, K., "Visualization of Pulsed Vortex Generator Jets for Active Control of Boundary Layer Separation," 28th AIAA Fluid Dynamic Conference, AIAA Paper 97-2021, June 1997.

[10] Liu, M. Y., Sankar, L. N., Englar, R. J., Ahuja, K. K., and Gaeta, R., "Computational Evaluation of the Steady and Pulsed Jet Effects on the Performance of a Circulation Control Wing Section," 42nd AIAA Aerospace Sciences Meeting and Exhibit, AIAA Paper 2004-0056, Jan. 2004.

[11] Zha, G. C., and Paxton, C., "A Novel Airfoil Circulation Augment Flow Control Method Using Co-Flow Jet," *Applications of Circulation Control Technologies*, edited by R. D. Joslin and G. S. Jones, Progress in Aeronautics and Astronautics, Vol. 214, AIAA, Reston, VA, 2006, pp. 293–314.

[12] Zha, G.-C., Gao, W., and Paxton, C. D., "Numerical Simulation of Co-Flow Jet Airfoil Flows," 44th AIAA Aerospace Sciences Meeting and Exhibit Conference, AIAA Paper 2006-1060, Jan. 2006.

[13] Zha, G.-C., Gao, W., and Paxton, C. D., "Jet Effects on Co-Flow Jet Airfoil Performance," *AIAA Journal*, Vol. 45, No. 6, 2007, pp. 1222–1231. doi:10.2514/1.23995

[14] Paxton, C., Zha, G.-C., and Car, D., "Design of the Secondary Flow System for a Co-Flow Jet Cascade," 40th AIAA/ASME/SAE/ASEE Joint Propulsion Conference and Exhibit, AIAA Paper 2004-3928, July 2004.

[15] Tangemann, R., and Gretler, W., "The Computation of a Two-Dimensional Turbulent Wall Jet in an External Stream," *Journal of Fluids Engineering*, Vol. 123, No. 1, 2001, pp. 154–157. doi:10.1115/1.1331557

[16] Launder, B. E., and Rodi, W., "The Turbulent Wall Jet," *Progress in Aerospace Sciences*, Vol. 19, 1979, pp. 81–128. doi:10.1016/0376-0421(79)90002-2

[17] Ekaterinaris, J. A., "Prediction of Active Flow Control Performance on Airfoils and Wings," *Aerospace Science and Technology*, Vol. 8, No. 5, 2004, pp. 401–410. doi:10.1016/j.ast.2004.02.003